NeuroImage: Clinical 36 (2022) 103245

Contents lists available at ScienceDirect

NeuroImage: Clinical

journal homepage: www.elsevier.com/locate/ynicl

Frequency-dependent white-matter functional network changes associated with cognitive deficits in subcortical vascular cognitive impairment

Juanwei Ma [a,b,c,d,e,1], Feng Liu [e,1], Yang Wang [e], Lin Ma [e], Yali Niu [f], Jing Wang [f], Zhaoxiang Ye [a,b,c,d,*], Jing Zhang [e,*]

[a] Department of Radiology, Tianjin Medical University Cancer Institute and Hospital, Tianjin, China
[b] National Clinical Research Center for Cancer, Tianjin, China
[c] Key Laboratory of Cancer Prevention and Therapy, Tianjin, China
[d] Tianjin's Clinical Research Center for Cancer, Tianjin, China
[e] Department of Radiology and Tianjin Key Laboratory of Functional Imaging, Tianjin Medical University General Hospital, Tianjin, China
[f] Department of Rehabilitation, Tianjin Medical University General Hospital, Tianjin 300052, China

ARTICLE INFO

Keywords:
White matter functional network
Vascular cognitive impairment
Functional connectivity
Amplitude
fMRI

ABSTRACT

Vascular cognitive impairment (VCI) refers to all forms of cognitive decline associated with cerebrovascular diseases, in which white matter (WM) is highly vulnerable. Although previous studies have shown that blood oxygen level-dependent (BOLD) signals inside WM can effectively reflect neural activities, whether WM BOLD signal alterations are present and their roles underlying cognitive impairment in VCI remain largely unknown. In this study, 36 subcortical VCI (SVCI) patients and 36 healthy controls were enrolled to evaluate WM dysfunction. Specifically, fourteen distinct WM networks were identified from resting-state functional MRI using *K*-means clustering analysis. Subsequently, between-network functional connectivity (FC) and within-network BOLD signal amplitude of WM networks were calculated in three frequency bands (band A: 0.01–0.15 Hz, band B: 0.08–0.15 Hz, and band C: 0.01–0.08 Hz). Patients with SVCI manifested decreased FC mainly in bilateral parietal WM regions, forceps major, superior and inferior longitudinal fasciculi. These connections extensively linked with distinct WM networks and with gray-matter networks such as frontoparietal control, dorsal and ventral attention networks, which exhibited frequency-specific alterations in SVCI. Additionally, extensive amplitude reductions were found in SVCI, showing frequency-dependent properties in parietal, anterior corona radiate, pre/post central, superior and inferior longitudinal fasciculus networks. Furthermore, these decreased FC and amplitudes showed significant positive correlations with cognitive performances in SVCI, and high diagnostic performances for SVCI especially combining all bands. Our study indicated that VCI-related cognitive deficits were characterized by frequency-dependent WM functional abnormalities, which offered novel applicable neuromarkers for VCI.

1. Introduction

Vascular cognitive impairment (VCI) is the second most common cause of clinically diagnosed dementia following Alzheimer's disease, ranging from subjective cognitive decline, mild cognitive decline to full-blown dementia (O'Brien et al., 2003; van der Flier et al., 2018). Various cerebrovascular diseases contribute to VCI, such as small vessel disease, large artery atherosclerosis, and brain hemorrhages. Chronic cerebral hypoperfusion (CCH), as a result of vascular diseases, are critical drivers of pathogenic mechanisms in VCI. White matter (WM) was considered to be highly vulnerable to CCH due to less metabolic reserve and relative hypoperfusion than gray matter (GM) (Iadecola 2013). WM damages are a significant contributor to cognitive impairment and the main pathological features of VCI, characterized by hyperintensities and infarcts on MRI (Kalaria, 2016; van der Flier et al., 2018). Microscopically, WM damages are primarily formed from axonal demyelination that is usually

* Corresponding authors at: Department of Radiology, Tianjin Medical University General Hospital, No. 154, Anshan Road, Heping District, Tianjin 300052, China (J. Zhang). Department of Radiology, Tianjin Medical University Cancer Institute and Hospital, Huan-Hu-West Road, Ti-Yuan-Bei, Hexi District, Tianjin 300060, China (Z. Ye).
E-mail addresses: zye@tmu.edu.cn (Z. Ye), zhangjing1970@163.com (J. Zhang).
[1] Juanwei Ma and Feng Liu have contributed equally to this work.

https://doi.org/10.1016/j.nicl.2022.103245
Received 14 May 2022; Received in revised form 7 October 2022; Accepted 21 October 2022
Available online 25 October 2022

derived from the loss of oligodendrocytes and accompanied by glial activation and loss of axon-glial integrity (Masumura et al., 2001; Reimer et al., 2011; Barker et al., 2013; Holland et al., 2015), which have been observed in both patients and animal models with VCI (Kalaria, 2016; Trigiani et al., 2020). In addition, recent studies have demonstrated that WM pathology severity was correlated with cognitive impairment and dementia (Boyle et al., 2016; Kantarci et al., 2017). Therefore, assessing WM dysfunction and characterizing its underlying pathological correlates would be critical for managing and preventing VCI.

Diffusion tensor imaging and other similar neuroimaging techniques have allowed for great strides to be made in our understanding of the structural integrity and connectivity patterns of WM (Gao et al., 2012a; Gao et al., 2012b; Zhang et al., 2014; He et al., 2022; Zhang et al., 2022). In VCI, these approaches have been widely used to probe WM structural abnormalities by combining voxel-wise (Mascalchi et al., 2019), region-of-interest (Qin et al., 2021), and graph-theoretical analyses (Tuladhar et al., 2016). These studies have mainly evaluated the structural abnormalities of WM, however, they failed to uncover any functional changes within the WM region in VCI.

Over the past two decades, resting-state functional MRI (fMRI) has become a promising technique to assess the brain's intrinsic activity of the GM in physiological status and various neuropsychiatric disorders (Biswal et al., 1995; Liu et al., 2013). Recently, several studies have demonstrated that blood oxygen level-dependent (BOLD) signals within WM can be detected and effectively reflect specific neural activities (Ji et al., 2017; Ding et al., 2018; Liu et al., 2017; Xue et al., 2020). In addition, Peer and colleagues identified symmetric WM functional networks in BOLD signals during the resting state, similarly to the GM (Peer et al., 2017). Li et al. further quantified the functional importance of individual WM voxels using engagement (Li et al., 2020). To date, WM functional abnormalities have been demonstrated to characterize the underlying pathological processes of many brain disorders including schizophrenia (Fan et al., 2020), bipolar disorder (Lu et al., 2021), and autism spectrum disorder (Ma et al., 2022). Therefore, it is feasible to characterize the WM dysfunction in VCI using fMRI.

Functional connectivity (FC), measuring the temporal interaction between spatially distinct brain areas, was taken as a crucial indicator for estimating brain connectivity and further diagnosing brain diseases Woodward and Cascio, 2015; Liu et al., 2015. Recently, FC has been reported to track BOLD signal correlations in WM and be associated with the pathological conditions such as mild cognitive impairment (Chen et al., 2017), Alzheimer's disease (Makedonov et al., 2016), and epilepsy (Jiang et al., 2019b). In addition to the FC, power spectral analysis of signals, depicting the intensity of BOLD signals in component frequencies (Zou et al., 2008), was considered as an alternative approach to characterize the features in interest. Up to now, power spectral analysis has been widely employed to discover the significant differences in the signal amplitude between different pathophysiologic conditions or different brain regions in GM (Yang et al., 2007; Zuo et al., 2010). Thus, making explicit the between-region functional interactions and within-region spontaneous activities in WM functional networks may facilitate the illustration of the pathological mechanisms in VCI.

Here, to evaluate WM dysfunction of VCI, we investigated WM functional networks using resting-state fMRI in 36 patients with subcortical VCI (SVCI) and 36 healthy controls (HCs). First, the WM functional networks were constructed via *K*-means clustering approach based on the WM voxel-wise correlation matrix. Second, considering that different frequency bands depict distinct physiological status and specific-disorder alterations (Han et al., 2011), the entire frequency range was divided into two sub-bands as previously suggested (Jiang et al., 2019a). The FC and signal amplitudes of WM were evaluated in each sub-band and the whole band. Third, we investigated the relationships between WM functional networks changes with cognitive variables. Finally, we constructed a WM network-based classification model to separate SVCI patients from HCs. We hypothesized that WM functional networks would exhibit frequency-dependent disruptions in SVCI, and these disruptions would be correlated with patients' cognitive performances and be neuromarkers for the early diagnosis of VCI.

2. Materials and methods

2.1. Subjects

The study was approved by the Research Ethics Committee of Tianjin Medical University General Hospital, and signed informed consent was obtained from all participants. In total, 36 SVCI patients were recruited and diagnosed by two trained neurological physicians based on the following criteria: (1) subjective cognitive complaint by patients or their caregivers for at least 3 months; (2) objective cognitive impairment in at least one domain regarding visuospatial, executive, memory, and language function on neuropsychological tests; (3) subcortical small infarcts ($\leq$ 20 mm in diameter) with/without WM hyperintensities on brain MRI scans; (4) Hachinski Ischemic Score $\geq$ 7; (5) focal neurologic signs or symptoms. Exclusion criteria included: (1) pre-existing cognitive impairment; (2) a history of hemorrhagic stroke, traumatic brain injury, Parkinson disease, psychiatric disorders or cortical infarct affecting cognitive function; (3) acute-phase cerebrovascular disease; (4) gross morphological anomalies on brain MRI scans. In addition, 36 age-, gender- and education-matched HCs were recruited from local community, and they were interviewed to confirm: (1) no history of known neurologic or psychiatric disorders; (2) normal cognitive function determined by neuropsychological tests.

All participants underwent brain MRI scans and neuropsychological tests. Specifically, the Mini-Mental State Examination (MMSE) and Montreal Cognitive Assessment (MoCA) were used to evaluate their cognitive function The schematic flowchart of this study was shown in Fig. 1.

2.2. Data acquisition

The MRI data were obtained using a 3.0 Tesla Siemens Prisma MR scanner equipped with a 64-channel head coil at Tianjin Medical University General Hospital. Foam paddings and soft earplugs were utilized to minimize head movement and reduce scanner noise, respectively. During data acquisition, all subjects were instructed to remain awake and think of nothing. High-resolution T1-weighted anatomical images were acquired by a magnetization-prepared rapid gradient-echo sequence as follows: repetition time (TR) = 2000 ms, echo time (TE) = 2.26 ms, inversion time = 900 ms, flip angle (FA) = 8°, field of view (FOV) = 256 × 256 mm^2, voxel size = 1 × 1 × 1 mm^3, matrix = 256 × 256, slice thickness = 1 mm, 192 sagittal slices, and no gap. Resting-state functional images were acquired by a single-shot echo-planar-imaging sequence with the parameters: TR = 750 ms, TE = 30 ms, FA = 54°, FOV = 222 × 222 mm^2, voxel size = 3 × 3 × 3 mm^3, matrix = 74 × 74, slice thickness = 3 mm, 48 axial slices, and 640 volumes.

2.3. Data preprocessing

Resting-state functional images were preprocessed using the Data Processing Assistant for Resting-State fMRI (DPARSF, https://rfmri.org/DPARSF), Statistical Parametric Mapping toolkits (SPM12, https://www.fil.ion.ucl.ac.uk/spm) and open MATLAB scripts (https://mind.huji.ac.il/white-matter.aspx) (Peer et al., 2017). Briefly, the fMRI scans were first realigned to the mean functional image to correct for head motion. Participants with maximum motion > 3 mm translation or 3° rotation were excluded. For each subject, T1-weighted anatomical images were then co-registered with the mean motion-corrected functional images, and further segmented into tissue probability maps of GM, WM, and cerebrospinal fluid (CSF). Based on segmented images, the normalization parameters from native space to Montreal Neurological Institute (MNI) standard space were estimated using DARTEL algorithm

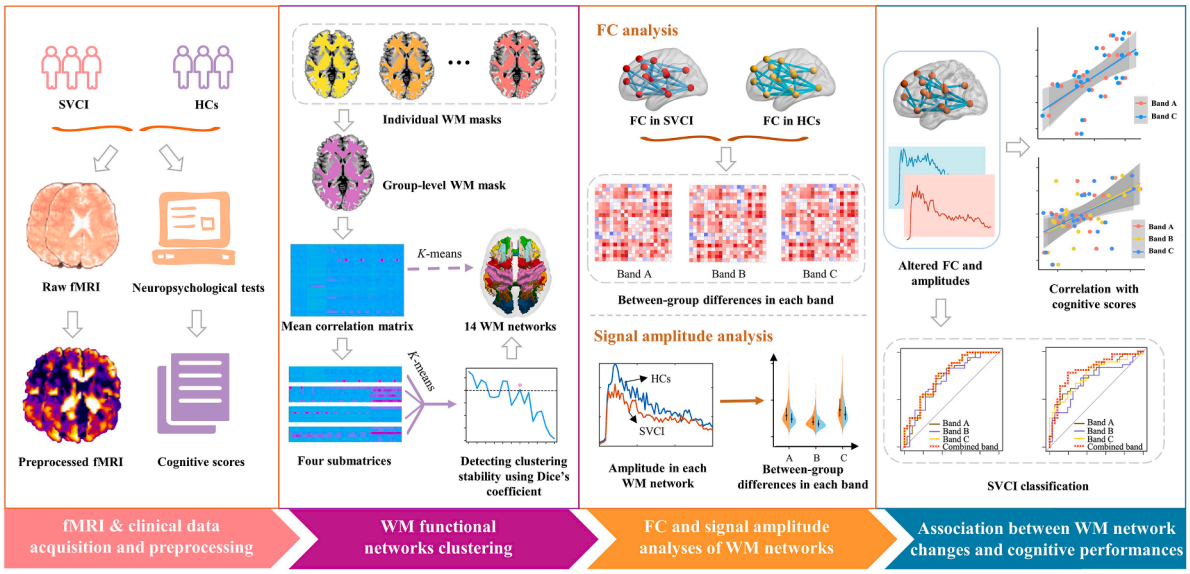

Fig. 1. Schematic flowchart of this analysis. Band A, 0.01–0.15 Hz; band B, 0.08–0.15 Hz; band C, 0.01–0.08 Hz. **Abbreviations:** FC, functional connectivity; fMRI, functional magnetic resonance imaging; HCs, healthy controls; SVCI, subcortical vascular cognitive impairment; WM, white matter.

(Ashburner 2007). Subsequently, several nuisance covariates were regressed out, including linear drift, mean CSF signals, and Friston-24 head motion parameters (Friston et al., 1996). To avoid eliminating signals of interest, WM and global brain signals were not regressed from the BOLD signals (Peer et al., 2017; Jiang et al., 2019a). Next, a band-pass filtering (0.01–0.15 Hz) was performed to minimize high-frequency non-neuronal noise sources in accordance with prior WM functional network studies (Jiang et al., 2019a; Wang et al., 2020). To avoid partial volume effect, the functional images were smoothed separately for WM and GM with a Gaussian kernel of 4-mm full width at half-maximum. Specifically, individual WM or GM voxels were identified using a 50 % threshold on above-mentioned GM/WM probability maps for each subject (Peer et al., 2017). Finally, the functional images were normalized to MNI space using the normalization parameters and resampled to a voxel size of $3 \times 3 \times 3$ mm^3.

2.4. Clustering WM functional networks

To investigate WM functional networks, group-level WM mask was first generated with subsequent procedures: (1) individual WM mask was first obtained according to the T1 anatomical image segmentation results; (2) individual WM mask was then averaged across all subjects and voxels identified as WM in $>$ 60 % of all participants were utilized for group-level WM mask creation (Peer et al., 2017; Wang et al., 2020); (3) we removed voxels identified as WM or GM without having functional data in $>$ 80 % of the subjects, for instance, parts of the medulla, spinal cord and cerebellum; (4) the subcortical structures were removed from the group-level WM mask as these areas had been erroneously identified as WM (Desikan et al., 2006; Babalola et al., 2009; Lorio et al., 2016). Finally, the group-level WM mask (included 15354 voxels) was obtained.

To cluster WM functional networks within group-level WM areas, voxel-level correlation matrix should be calculated. Considering the computational complexity, an interchanging grid method was used to subsample the WM mask (Peer et al., 2017; Jiang et al., 2019a). Pearson's correlation coefficient was calculated between all of the WM voxels and each subsampled WM voxel, resulting in a correlation matrix (15354×3840) for each participant (Yeo et al., 2011; Craddock et al., 2012). *K*-means clustering algorithm was carried out on the mean correlation matrix across all subjects (MATLAB "kmeans" function with the options of distance measure: correlation and replicates: 10) (Blumensath et al., 2013; Yeo et al., 2014), clustering all the WM voxels into *K* independent spatial networks. To detect the most stable number of WM networks, the stability of the clustering solution was evaluated for each number of clusters (*K*) ranging from 2 to 22 (Lange et al., 2004; Yeo et al., 2011). Specifically, the mean correlation matrix (15354×3840) was randomly divided into four subgroups (15354×960). The same clustering approach was performed on each submatrix separately; the clustering showing approximately similar pattern on each subgroup represented stable clustering solutions (Lange et al., 2004; Yeo et al., 2011). As *K*-means clustering attached random labels to clusters, there was difficulty in similarity evaluation in clustering solutions between subgroups. Thus, adjacency matrix was utilized to measure the between-subgroup similarity of the clustering results, and these adjacency matrices were compared using Dice's coefficient for all subgroup pairs. The average Dice's coefficient was acquired for each *K* and used to select the most stable number of WM networks.

In addition, to assess the symmetry of identified WM functional networks, we compared the clustering solutions for two hemispheres via Dice's coefficient. First, the half of the clustering whole-WM networks were flipped along the midsagittal plane to identify the clustering results in each hemisphere. Second, adjacency matrices were calculated for each hemisphere separately. Third, the clustering results were compared using Dice's coefficient across the two hemispheres. Fourth, a permutation test was performed to measure the significance of the symmetry values. Specifically, the *P* value was obtained after the adjacency matrix in each hemisphere was randomly permuted 5000 times.

2.5. FC and signal amplitude of WM functional networks

Considering frequency-dependent properties of the FC and signal amplitude (Salvador et al., 2005; Jiang et al., 2019b), the full band range (band A: 0.01–0.15 Hz) was further divided into two sub-bands (band B: 0.08–0.15 Hz and band C: 0.01–0.08 Hz) (Jiang et al., 2019a). The FC and amplitude were computed in each sub-band and the whole band.

To obtain the FC of WM functional networks, the Pearson's correlation coefficient between the mean time series of any two WM functional networks was calculated for each subject in each band. In addition, we also calculated the FC between each WM and GM functional networks, and between distinct GM functional networks to

examine functional interaction and differences between WM and GM. Given the existence of reliable and repeatable clustering networks within GM voxels (Yeo et al., 2011; Schaefer et al., 2018), we directly utilized the 7-network parcellation atlas to define GM functional networks (Yeo et al., 2011; Schaefer et al., 2018). The original FC was transformed to the z-scores using a Fisher's z transformation to improve data normality for further analyses. Moreover, considering that coarse parcellation schemes of GM may lead to the aggregation of signals from distinct functional regions, we also utilized a high-resolution parcellation with Yeo's 17 GM network atlas to define GM networks, and to further assess the FC alterations in patients with SVCI. The above internetwork FC calculation procedures were repeated for the high-resolution GM parcellation scheme.

Existing studies have found that low-frequency oscillatory amplitude was a sensitive and reliable neurophysiologic index and related to spontaneous neural activities in the resting state (Fox & Raichle, 2007). In the current study, the power spectral frequency distribution of the amplitude was calculated by the Fourier transform in each WM network. Moreover, individual averaged amplitude in each WM network was computed and compared between the SVCI and HCs group for band A, B and C. To avoid the partial volume effect, only individual WM or GM voxels identified based on the T1 image segmentation results were used for signal averaging in FC and amplitude analyses.

2.6. Statistical analyses

Chi-square test was performed to test the differences in gender, and two-sample *t*-tests were performed to test the differences in age, education, and cognitive test scores between the SVCI and HCs group.

The network-based statistic (NBS) approach was utilized to identify the clustering structures of FC alterations in SVCI (Zalesky et al., 2010). A cluster-defining primary threshold ($P = 0.05$) was first applied to identify a set of connected components controlling for the effects of age and gender, in which each component size (number of edges) was then determined. To assess the significance for each component, the empirical null distribution of the maximal connected component size was derived using a permutation test (5000 permutations). For a component of size M obtained in the original data, the corrected P value was estimated as the proportion of permutations that the maximal component sizes were greater than or equal to M. All the aforementioned steps were conducted using the NBS software package (https://www.nitrc.org/projects/nbs/).

In addition, to determine the effects of group and frequency band on signal amplitude, we performed a two-way mixed analysis of variance (ANOVA) with group (SVCI and HCs) as a between-subject factor and frequency band (band A, B and C) as a within-subject factor. Multiple comparisons were corrected by the Benjamini-Hochberg false discovery rate (BH-FDR) method at the $P < 0.05$ level. Then, for those WM networks with significant main effects of group and interaction between group and frequency band, post-hoc two-sample *t* tests were carried out to detect group differences in signal amplitudes, with BH-FDR for multiple comparison correction ($P < 0.05$). Of note, before the mixed ANOVA, a linear regression model was applied to remove the effects of age and gender.

Moreover, to examine whether the WM network alterations were associated with cognitive performances in SVCI, the partial correlation coefficient was calculated between altered functional connections and signal amplitudes and cognitive test scores (MMSE and MoCA scores) for each band in SVCI group, regarding age and gender as covariates. $P < 0.05$ was considered significant.

Furthermore, a step-wise logistic regression model and receiver operator characteristic (ROC) curve analyses were performed to test whether FC and signal amplitudes can be used to discriminate SVCI patients from HCs. Specifically, the FC and amplitude values were first extracted between each significant pair of networks and within each significant network, respectively. Subsequently, these extracted values were entered into step-wise logistic regression and ROC curve analyses to investigate their diagnostic values in each frequency band, while removing the effects of age and gender. In addition, to explore whether the complementary information of distinct frequency bands would improve the results, the extracted values of FC and amplitudes of all bands (band A, B and C) were separately combined into the above-mentioned predictive model. The significance level was set at $P < 0.05$ in the classification analyses.

2.7. Validation analyses

To verify the reproducibility of the results, a split-half approach was first conducted (Zhang et al., 2011). Briefly, both the SVCI and HCs group were divided into two matched subgroups (**Table S1**), and no significant differences were observed in the age and gender between two subgroups (HC1 and HC2, SVCI1 and SVCI2) (all $Ps > 0.72$). To identify whether there was a similar data distribution in the subgroups, Pearson's correlation coefficients were separately computed for the FC and amplitude between HC1 and HC2 subgroups and between SVCI1 and SVCI2 subgroups. Then, the significantly different functional connections and amplitudes obtained from the whole-group analysis were compared between two subgroups (HC1 and SVCI1, HC2 and SVCI2), and the same correlation and predictive analyses were performed.

Furthermore, we performed additional analyses to further examine the consistency of the results. In the current study, a threshold of 50 % through SPM12′s tissue segmentation was used to generate an individual-level WM mask, and the threshold of percentage > 60 % was used to generate a group-level WM mask, which was in line with prior studies (Jiang et al., 2019a; Jiang et al., 2019b; Lu et al., 2021). Furthermore, another three individual-level (40 %, 60 %, and 70 %) and three group-level (50 %, 70 %, and 80 %) thresholds were utilized to validate the consistency of the main results.

Finally, to verify the impact of head motion and motion correction strategies on these WM network metrics in the resting state, additional analyses were carried out. Specifically, scrubbing was performed using head motion "spikes" (identified by framewise displacement > 1 mm, along with 1 preceding and 2 subsequent volumes) as separate regressors. With scrubbing, we also performed the clustering of the WM functional networks, FC and signal amplitude analyses, and correlation and predictive analyses. All these validation analyses were carried out while controlling for the effects of age and gender.

3. Results

3.1. Demographics and clinical characteristics of the participants

The results indicated that the two groups were well-matched for gender (23 males for the SVCI and 15 males for the HCs; $P = 0.059$), age (57.94 ± 6.60 years for the SVCI and 57.25 ± 6.60 years for the HCs; $P = 0.657$), and education (11.50 ± 3.40 years for the SVCI and 13.00 ± 2.72 years for the HCs; $P = 0.061$). The significantly lower MMSE ($P < 0.001$) and MoCA scores ($P < 0.001$) were observed in SVCI group compared with HCs. Details of demographics and clinical information on the subjects were provided in Table 1.

3.2. Identification of WM functional networks

The WM functional networks were determined using unsupervised *K*-means clustering on the group-level mean correlation matrix. The clustering results showed 14 was the largest number of WM networks with a high stability (Dice's coefficient > 0.85) (**Fig. S1**), which was chosen for the further analysis. The detailed information regarding the 14 WM networks was depicted in Fig. 2 **and Table S2**. These WM functional networks showed relatively high symmetry (permutation test $P < 0.0002$; Dice's coefficient = 0.72), correlated with several known WM tracts and were organized into three layers (superficial, middle and

Table 1
Demographics and clinical characteristics of the participants.

Variables	SVCI ($n = 36$) (Mean ± SD)	HCs ($n = 36$) (Mean ± SD)	P value
Gender (male/female)	23/13	15/21	0.059[a]
Age (years)	57.94 ± 6.60	57.25 ± 6.60	0.657[b]
Education (years) *	11.50 ± 3.40 ($n = 36$)	13.00 ± 2.72 ($n = 28$)	0.061[b]
Cognitive test scores *			
MMSE	24.14 ± 3.88 ($n = 29$)	27.91 ± 2.45 ($n = 22$)	< 0.001[b]
MoCA	21.09 ± 4.73 ($n = 23$)	26.52 ± 4.03 ($n = 21$)	< 0.001[b]

[a] P value was acquired from a chi-square test; [b] P value was acquired by a two-sample t-test. * The education years and cognitive test scores of some subjects were missing. **Abbreviations:** HCs, healthy controls; MMSE, Mini-Mental State Examination; MoCA, Montreal Cognitive Assessment; SD, standard deviation; SVCI, subcortical vascular cognitive impairment.

deep), as reported previously (Peer et al., 2017; Jiang et al., 2019a).

3.3. Frequency-dependent FC changes of WM networks

The NBS analysis indicated extensive, frequency-dependent reduced functional connections in patients with SVCI, mainly linking distinct WM networks together with WM and GM networks. Specifically, in band A, NBS identified a single component showing significantly (corrected $P = 0.0456$) decreased connections in SVCI group. The component comprised 31 connections, involving 17 different networks. The involved networks encompassed the parietal (WM1), forceps major (WM2), pre/post central (WM4), posterior limb of internal capsule (WM5), superior corona radiate (WM6), frontotemporal parietal (WM9), superior longitudinal fasciculus (WM10), ventral frontal (WM11), dorsal frontal (WM12), inferior longitudinal fasciculus (WM13) and occipital (WM14) WM networks, along with visual (GM1), somatomotor (GM2), dorsal attention (GM3), ventral attention (GM4), frontoparietal control (GM6) and default mode (GM7) GM networks (Fig. 3**A**). Additionally, in band B, a single connected component consisting of 32 connections involved in 16 WM networks, including WM1, WM2, WM4, WM5, anterior limb of internal capsule (WM8), WM9, ventral frontal (WM11), WM12, WM13, GM1, GM2, GM3, GM4, limbic (GM5), GM6, and GM7 networks. Compared with the HCs, all of the connections in this band exhibited a significant decrease in the SVCI compared with the HCs (corrected $P = 0.0410$) (Fig. 3**B**). Furthermore, a disrupted connected component comprising 29 connections was identified in SVCI patients at the low-frequency range (0.01–0.08 Hz) (corrected $P = 0.0426$). These connections linked 15 WM networks, including the WM1, WM2, WM4, WM5, WM6, WM9, WM10, WM12, WM13, WM14, GM1, GM2, GM3, GM4, and GM6 networks. In band C, all impaired connections were significantly reduced in SVCI, and only connections between different WM networks and between WM and GM networks were involved excepting that between GM1 and GM3 (Fig. 3**C**). In addition, there were 27 significant altered connections overlapping between the band A and C, involving WM1, WM2, WM4, WM5, WM6, WM9, WM10, WM12, WM13, WM14, GM1, GM2, GM3, GM4, and GM6 networks, and 10 significant altered connections overlapping between band A and B consisting of WM1, WM2, WM4, WM9, WM11, WM12, GM2, GM3,

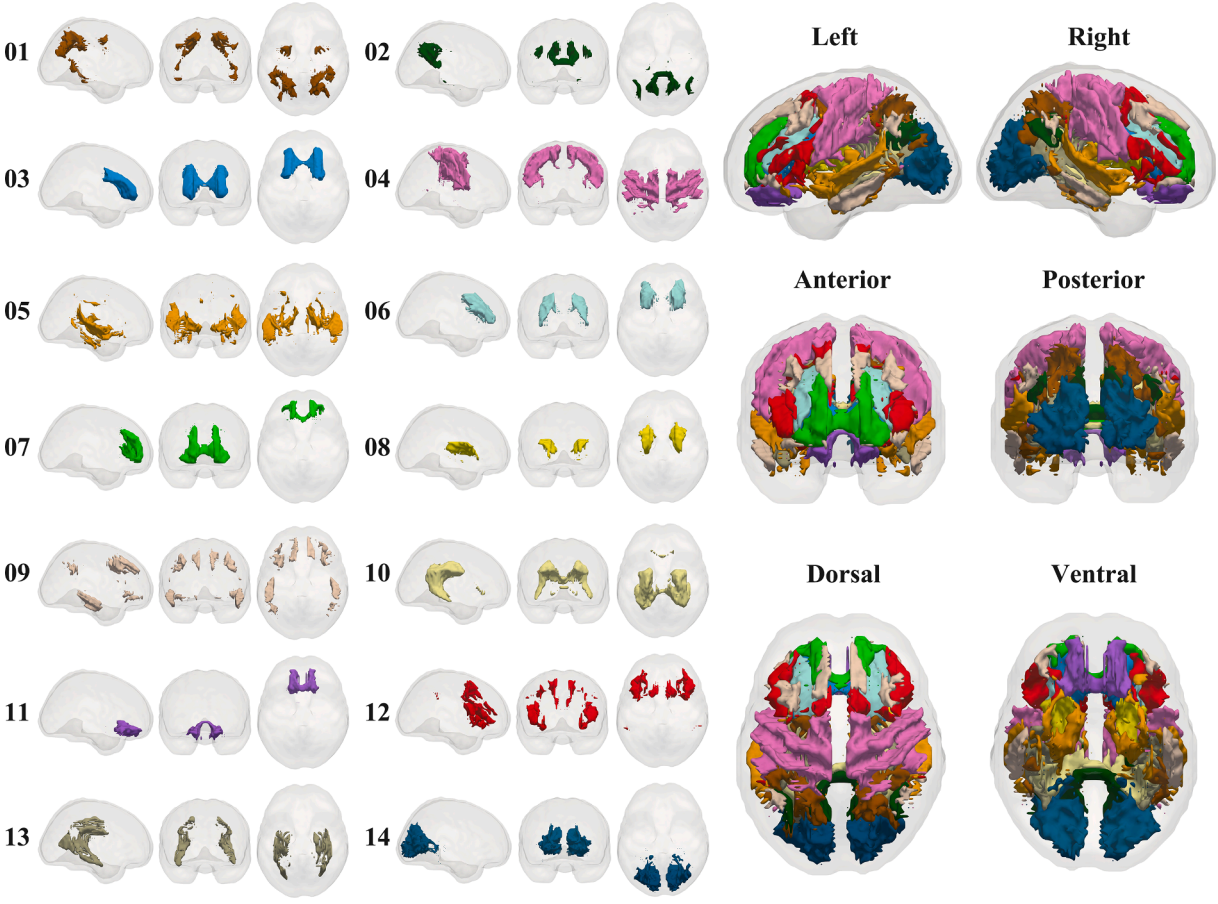

Fig. 2. White matter functional networks obtained using K-means clustering approach. 01. Parietal network; 02. Forceps major network; 03. Anterior corona radiate network; 04. Pre/post central network; 05. Posterior limb of internal capsule network; 06. Superior corona radiate network; 07. Forceps minor network; 08. Anterior limb of internal capsule network; 09. Frontotemporal parietal network; 10. Superior longitudinal fasciculus network; 11. Ventral frontal network; 12. Dorsal frontal network; 13. Inferior longitudinal fasciculus network; 14. Occipital network.

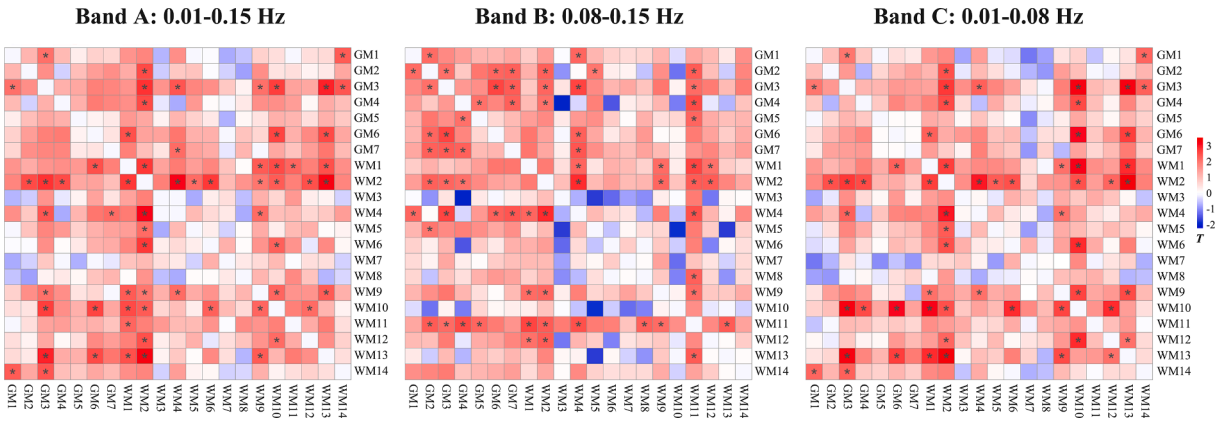

Fig. 3. Differences in FC between SVCI and HCs in three frequency bands. Left panel, significant differences of FC between SVCI and HCs group in band A (NBS corrected $P = 0.0456$). Middle panel, significant between-group differences of FC in band B (NBS corrected $P = 0.0410$). Right panel, significant differences of FC between SVCI and HCs group in band C (NBS corrected $P = 0.0426$). Significant differences after NBS correction are marked with a black asterisk in each band. The color bar represents the T values of between-group comparison. Band A, 0.01–0.15 Hz; band B, 0.08–0.15 Hz; band C, 0.01–0.08 Hz. **Abbreviations:** FC, functional connectivity; HCs, healthy controls; NBS, network-based statistic; SVCI, subcortical vascular cognitive impairment.

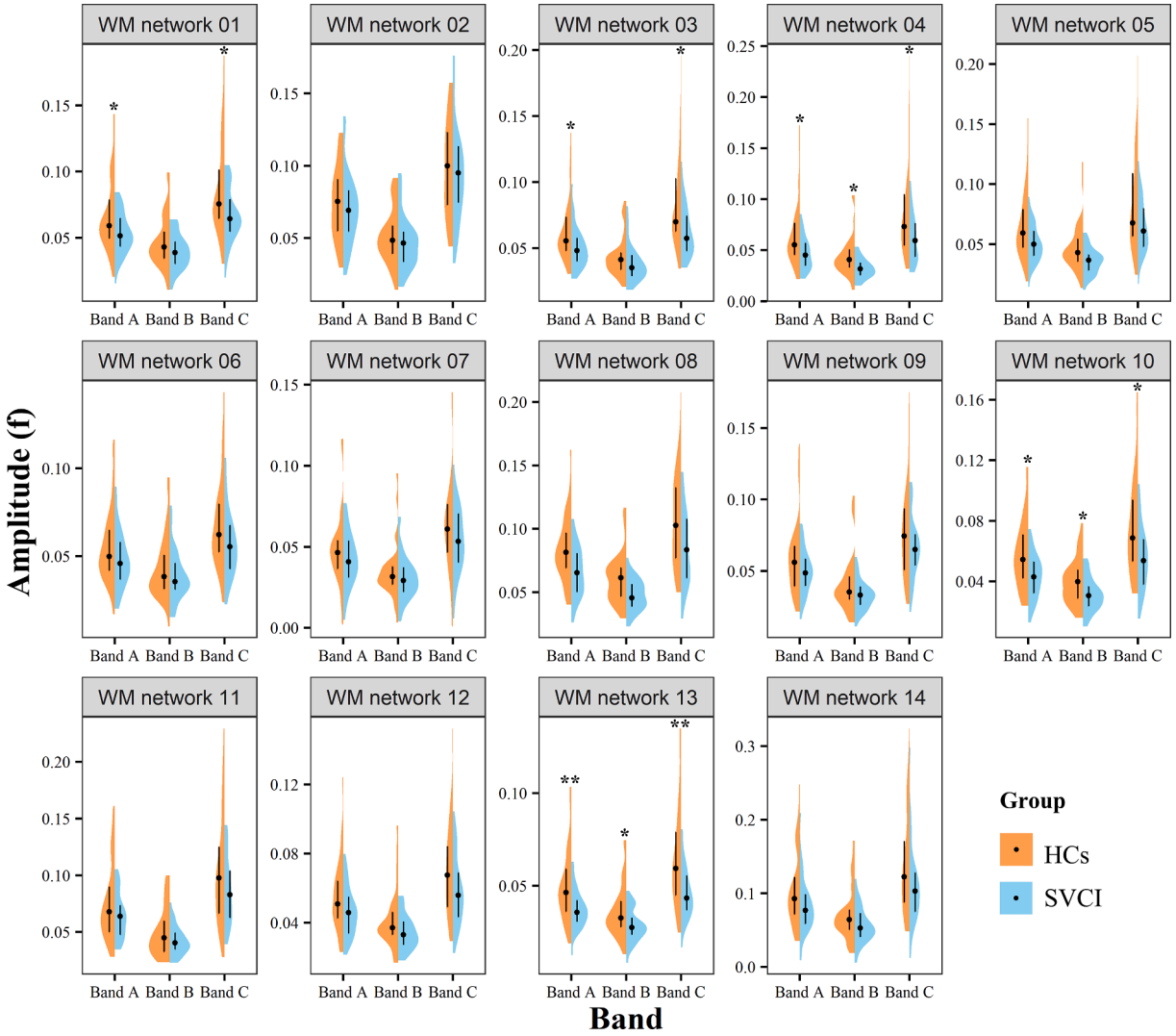

Fig. 4. Amplitude of WM functional networks. Violin plots show the differences of signal amplitude in each WM network and frequency band between SVCI and HCs group (controlling for age and gender). The violin plots contain vertical lines that represent inter-quartile ranges, and black dots on lines indicate the median values. The results were obtained using two-way mixed ANOVA and post hoc *t*-tests, and BH-FDR method was used to correct the multiple comparison correction. * BH-FDR corrected $P < 0.05$ and ** BH-FDR corrected $P < 0.01$. Band A, 0.01–0.15 Hz; band B, 0.08–0.15 Hz; band C, 0.01–0.08 Hz. **Abbreviations:** ANOVA, analysis of variance; BH-FDR, Benjamini-Hochberg false discovery rate; HCs, healthy controls; SVCI, subcortical vascular cognitive impairment; WM, white matter.

GM4, and GM7.

In addition, Yeo's 17 GM network atlas was also adopted to define the GM networks exploring FC alterations in SVCI with high-resolution GM network parcellation. Similar to the patterns found in the low-resolution GM network parcellation, FC obtained in the high-resolution GM network exhibited an extensive and frequency-dependent decrease in patients with SVCI, and these reduced connections mainly linked distinct WM networks together with WM and GM networks. All involved networks in band A, and most of these networks in band B and C with low-resolution GM network parcellation were also confirmed in the high-resolution FC analyses. The details are provided in **Supplementary Results**.

3.4. Frequency-dependent signal amplitude alterations of WM networks

All the WM networks showed higher spontaneous activity at low

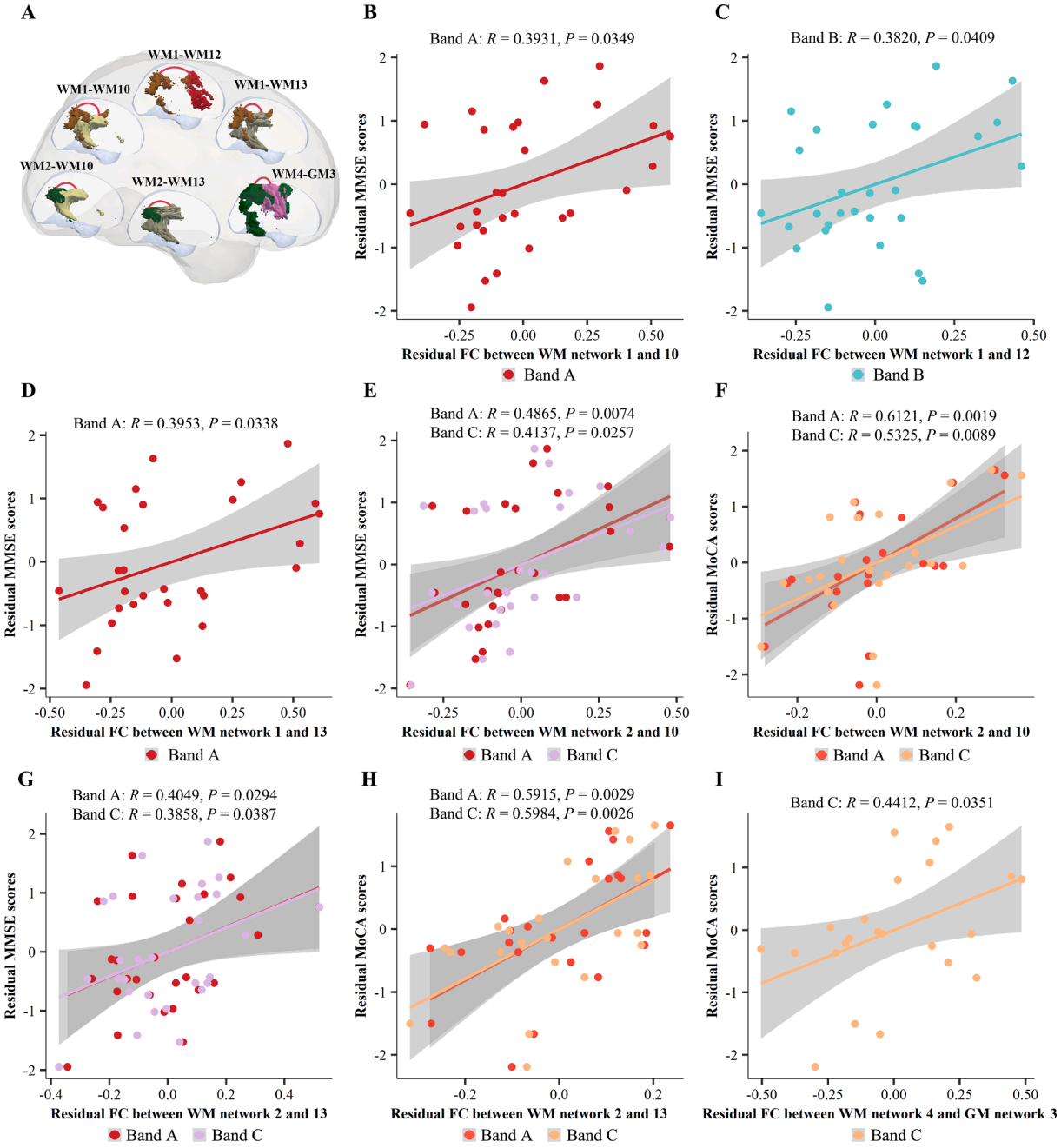

Fig. 5. Correlations between FC changes and cognitive performances in patients with SVCI. **(A)** Six WM functional connections (WM network 1 and 10, 1 and 12, 1 and 13, 2 and 10, 2 and 13, and WM network 4 and GM network 3) were positively correlated with cognitive performances. **(B)** FC between WM network 1 and 10 was positively associated with MMSE scores in band A. **(C)** FC between WM network 1 and 12 was positively associated with MMSE scores in band B. **(D)** FC between WM network 1 and 13 was positively associated with MMSE scores in band A. **(E–F)** In band A and C, FC between WM network 2 and 10 was positively associated with MMSE and MoCA scores. **(G–H)** In band A and C, FC between WM network 2 and 13 was positively associated with MMSE and MoCA scores. **(I)** FC between WM network 4 and GM network 3 was positively associated with MoCA scores in band C. The *R* and *P* values were obtained from partial correlation analyses. None of these correlations did not survive BH-FDR correction (corrected *P* values not shown). Band A, 0.01–0.15 Hz; band B, 0.08–0.15 Hz; band C, 0.01–0.08 Hz. **Abbreviations:** FC, functional connectivity; MMSE, Mini-Mental State Examination; MoCA, Montreal Cognitive Assessment; SVCI, subcortical vascular cognitive impairment; WM, white matter.

frequencies, with a decrease in signal amplitude at higher frequencies (Fig. S3). Variance analysis indicated WM networks showing a significant main effect for group were located in WM1, anterior corona radiate (WM3), WM4, WM5, WM8, WM10 and WM13 networks, where the amplitudes were decreased within the SVCI group. Moreover, significant interaction between group and frequency band on amplitudes were found in the WM1, WM3, WM4, WM10 and WM13 networks. Further post-hoc *t* test indicated that between-group differences in amplitudes were as follows, the most significant reduction in band C (0.01–0.08 Hz), the second in band A (0.01–0.15 Hz), and the least significant decrease in band B (0.08–0.15 Hz) for patients with SVCI (Fig. 4).

3.5. Relationship between impaired WM functional networks and cognitive performances

We performed partial correlation analyses to evaluate the relationship between altered WM functional network properties, including functional connections and signal amplitudes, and cognitive scores in the SVCI group. Five connections (WM1-WM10 and WM1-WM13 in band A; WM1-WM12 in band B; WM2-WM10 and WM2-WM13 in both band A and C) were positively correlated with MMSE scores in patients with SVCI (Fig. 5**A–E** and Fig. 5**G**). Moreover, three connections (WM2-WM10 and WM2-WM13 in both band A and C; WM4-GM3 in band C) were positively associated with MoCA scores (Fig. 5**A, F, H,** and **I**). In band B, only one connection (WM1-WM12) was significantly correlated with MMSE scores, and no correlation was observed between any altered connection and MoCA scores. In addition, signal amplitudes in 3 WM networks (WM3 in band A, B and C; WM4 and WM8 in band A and C) were positively correlated with MoCA scores in SVCI group (Fig. 6**A–D**), while none of amplitudes was associated with MMSE scores within all frequency band. However, none of the aforementioned correlations were found to be statistically significant after BH-FDR correction for multiple comparisons, which may be due in part to the small sample size.

3.6. Classification performance based on changed WM functional networks

We conducted ROC analysis and used area under the curve (AUC) to evaluate the discriminatory power of significant altered functional connections and signal amplitudes for diagnosing SVCI. Specifically, the AUC for functional connections was 0.7022 in band A, 0.6759 in band B, and 0.7631 in band C (all *Ps* < 0.05) (Fig. 7**A**). By considering all bands together, the AUC for functional connections reached 0.7963 (*P* < 0.001), which is higher than when each band was considered separately (Fig. 7**A**). Furthermore, we used the same procedure to discriminate SVCI patients from HCs by using signal amplitudes of WM networks. The findings indicated that the AUC of significant signal amplitudes in WM networks were relatively high (band A, 0.7106; band B, 0.7130; band C, 0.7531; combined band, 0.7531; all *Ps* < 0.01) (Fig. 7**B**). Therefore, the functional connections and signal amplitudes identified by our method, especially in the combined band, could be used as biomarkers for the

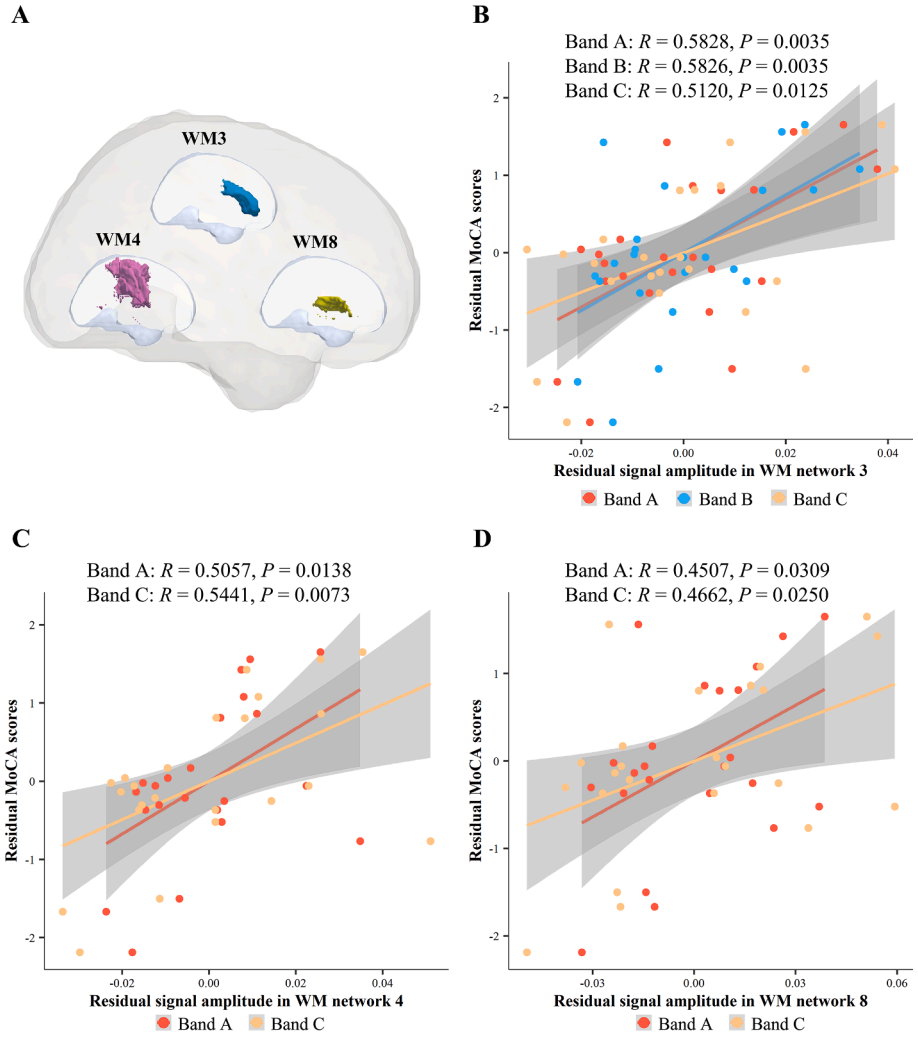

Fig. 6. Correlations between altered signal amplitudes of WM functional network and cognitive performances in patients with SVCI. **(A)** Signal amplitudes in three WM functional networks (WM network 3, 4, and 8) were positively associated with MoCA scores. **(B)** Signal amplitude in WM network 3 was positively correlated with MoCA scores in band A, B, and C. **(C–D)** Signal amplitudes in WM network 4 and 8 were positively correlated with MoCA scores in both band A and C. The *R* and *P* values were obtained from partial correlation analyses. None of these correlations did not survive BH-FDR correction (corrected *P* values not shown). Band A, 0.01–0.15 Hz; band B, 0.08–0.15 Hz; band C, 0.01–0.08 Hz. **Abbreviations:** MoCA, Montreal Cognitive Assessment; SVCI, subcortical vascular cognitive impairment; WM, white matter.

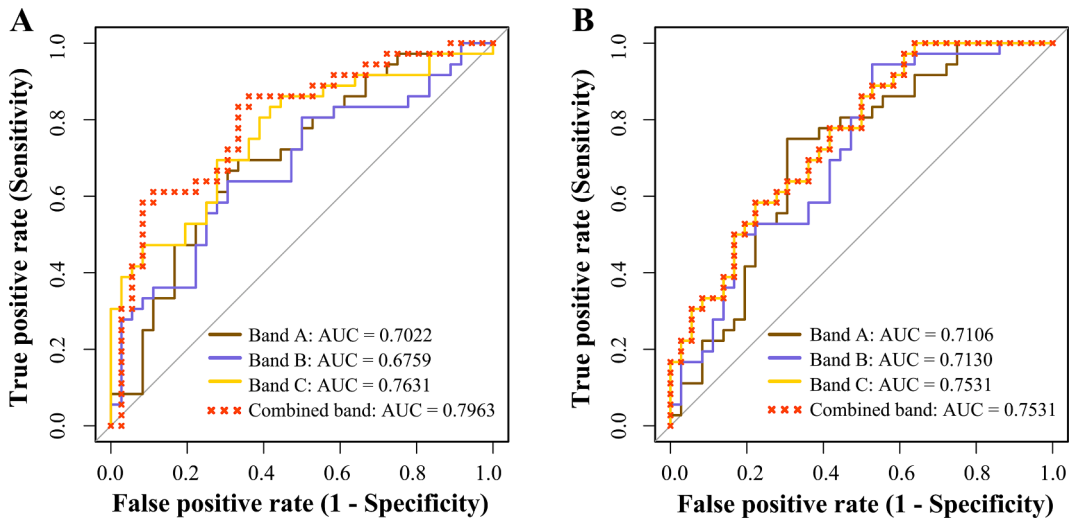

Fig. 7. ROC curves for classification of SVCI and HCs using altered functional connections and signal amplitudes. **(A)** Altered functional connections in each of 3 bands and the combined band (combining band A, B and C) were used to differentiate SVCI from HCs. The AUC for the combined band is higher than those for any single band. **(B)** Changed WM signal amplitudes in each of 3 bands and the combined band (combining band A, B and C) were used to distinguish SVCI from HCs. The AUC values for the combined band and for band C were equal, and their ROC curves completely overlapped. Band A, 0.01–0.15 Hz; band B, 0.08–0.15 Hz; band C, 0.01–0.08 Hz. **Abbreviations:** AUC, the area under the curve; HCs, healthy controls; ROC, receiver operating characteristic; SVCI, subcortical vascular cognitive impairment.

clinical diagnosis of SVCI.

3.7. Validation analyses

The split-half results were largely consistent with our main results. Moreover, our main results suggested a high reproducibility in validation analyses with different individual-level (40 %, 60 %, and 70 %) and group-level (50 %, 70 %, and 80 %) thresholds to determine WM mask (please see **Supplementary Results**). Furthermore, the validation results with scrubbing (regression of head motion "spikes") were similar to the results without scrubbing (**Supplementary Results**).

4. Discussion

This study identified spatially independent WM functional networks using clustering analysis of resting-state fMRI signals as previously reported (Peer et al., 2017; Jiang et al., 2019b; Fan et al., 2020). These WM networks were correlated with several anatomically established WM structures. Compared with HCs, the SVCI group manifested between-network FC decreases and within-network signal amplitude reductions in WM, which both exhibited frequency-dependent properties. In addition, these FC and amplitude disruptions showed positive correlations with cognitive performances in SVCI, and high diagnostic performances for SVCI especially combining all bands. Overall, our study demonstrated that VCI-related WM dysfunction can be detected using WM functional network and used as applicable biomarkers for the diagnosis of VCI.

Previous studies suggested the multiple WM structural abnormalities in cognitive deficits and WM damage played a role in cognition dysfunction (Filley 2012; Thong et al., 2014; Chen et al., 2018). For VCI, selective involvement of frontal tracts has been recognized to underlie executive dysfunction, and frontal and parietal WM integrity has been correlated with executive and global cognitive function (Ai et al., 2014; Levit et al., 2020). Microstructural changes in bilateral forceps major, superior longitudinal fasciculus and inferior longitudinal fasciculus were also reported in prior VCI studies (Tu et al., 2017). Recently, BOLD signals from WM regions have been correlated with other WM and GM areas in the resting state, similarly to FC arising from GM regions (Gao et al., 2020). Our results demonstrated the WM-related FC disruptions, mainly including bilateral parietal, forceps major, superior longitudinal fasciculus, and inferior longitudinal fasciculus WM regions. In addition to FC disruptions within WM regions, this study also found SVCI patients had FC disruptions between WM and GM regions, which were mainly connected to frontoparietal control, dorsal and ventral attention GM networks. Moreover, with high-resolution GM network parcellation, patients with SVCI exhibited similar FC alteration patterns as those in the low-resolution parcellation. These findings showed that both within-WM and WM-GM functional interactions were disrupted in SVCI with high stability, supporting the important role of cortical-subcortical interactions in cognition and the disruption of cortical-subcortical pathways in SVCI (Mungas et al., 2001; Min et al., 2020).

In this study, the frequency effect in WM-related FC disruptions in SVCI could be viewed from these two aspects. First, several altered functional connections were not shared among distinct frequency bands (full-, high-, and low-frequency band), which implied SVCI-related FC changes were related to specific frequency bands. Second, despite extensive disrupted connections linking distinct GM regions in high-frequency band, except for GM1-GM3 connection, SVCI patients exhibited only WM-related FC (WM-WM and WM-GM) alterations at the low- and full-frequency ranges. The frequency sub-bands contained the disease-related alterations in the full frequency band but characterized more differences (Jiang et al., 2019a), and therefore, the above only WM-related FC alterations in SVCI were mainly due to connection changes in the low-frequency band. As BOLD signals reflected neuronal activities mainly in the low-frequency band (Logothetis et al., 2001), the finding confirmed that spontaneous brain activity alterations could be sensitively detected using WM-related FC disruptions.

In addition, we found that SVCI patients had significantly deceased signal amplitudes, which were located in the parietal, anterior corona radiate, pre/post central, anterior and posterior limb of internal capsule, superior and inferior longitudinal fasciculus WM networks. These areas are responsible for distinct functions, for instance, posterior limb of internal capsule is one of regions where myelination first began (Li et al., 2022). These findings verified WM dysfunction in SVCI, consistent with earlier studies reporting that BOLD-fMRI in the WM was useful in the clinical characterization of small vessel disease abnormalities (Makedonov et al., 2013). Structural alterations could yield BOLD signal changes in WM (Lin et al., 2020), in turn, altered BOLD signals may reveal impaired WM integrity in cognitive disorders. In addition, WM has been shown to exhibit plasticity, the activity-dependent capacity of

neurons to be modified, in normal and neurological individuals (Filley & Fields 2016), thus altered spontaneous activities in WM detected by fMRI may offer a powerful approach to uncover WM plasticity in SVCI. Furthermore, SVCI patients showed specific-frequency WM amplitude decreases and the most significant reduction in the low frequency band, which were similar to abnormal frequency-specific intrinsic neural oscillations within GM in patients with SVCI (Li et al., 2014).

There is increasing evidence that significant correlations between cognitive declines and extensive WM lesions such as parietal WM (Ai et al., 2014), forceps major (Zamboni et al., 2017), superior and inferior longitudinal fasciculus (Chen et al., 2018) in VCI and its risk factors. In the present study, five decreased functional connections were positively correlated with MMSE-detected cognitive deficit in patients with SVCI, and these connections linked parietal WM and superior longitudinal fasciculus, parietal WM and dorsal frontal, parietal WM and inferior longitudinal fasciculus, forceps major and superior longitudinal fasciculus, along with forceps major and inferior longitudinal fasciculus. Moreover, three connections linking forceps major and superior longitudinal fasciculus, forceps major and inferior longitudinal fasciculus, as well as pre/post central WM and dorsal attention GM network were positively associated with MoCA-detected cognitive performances in full and low frequency band. These positive correlations between WM-related connections and cognitive performances support previous findings, suggesting the reduction in inter-regional connections may engage in cognitive mechanisms in SVCI. Several altered connections, which were positively correlated with both MoCA and MMSE scores, highlighted inherent cognitive deficit-related WM functional connections in patients with SVCI. However, signal amplitude changes of WM networks were only correlated with MoCA scores in SVCI. This may be attributed to the fact that MMSE primarily detects general cognitive deficits, while MoCA is more sensitive for mild cognitive impairment, particularly in executive function, attention and delayed recall (Pendlebury et al., 2010).

Furthermore, we found that impaired WM functional connections and signal amplitudes exhibited relatively high diagnostic power for SVCI and combined-band AUC value were higher than or equal to the greatest individual prediction. These data suggested complementary information in distinct bands could improve the diagnostic performance for VCI.

Several limitations should be considered in this study. First, numerous studies have shown that BOLD signals within WM reflected specific neural activities (Gore et al., 2019; Li et al., 2021), however, the precise weighting of the neuron activity, spiking-related metabolic demands and hemodynamic factors contributing to the WM BOLD signals is still unclear. Future studies should further quantify signal changes in WM. Second, as WM tracts cross each other, the signal at a certain location may be a mixture from distinct functional systems (Tournier et al., 2004). The *K*-means clustering approach used in this study might not consider the fiber crossings, which need to be improved in the future. Third, etiological heterogeneity is a potential factor affecting brain functional and structural changes in individuals with VCI. This study did not subdivide the VCI group into subgroups with different vascular etiologies, studies with the larger sample size are needed to establish whether or not etiological heterogeneity affect WM dysfunction in VCI. Finally, due to the small sample size, this study was limited by the its statistical power to detect significant effects. Future studies with larger sample sizes will make conclusions more reliable.

5. Conclusions

This study investigated WM dysfunction in SVCI using resting-state fMRI. SVCI patients exhibited extensive WM functional injuries, mainly including widespread disrupted WM-WM and WM-GM functional connections as well as signal amplitudes in WM regions. Importantly, these abnormalities of WM function exhibited frequency-specific properties. Furthermore, these impaired FC and signal amplitudes were positively correlated with cognitive decline and exhibited high diagnostic performances for SVCI. In summary, this study demonstrates that VCI is associated with frequency-dependent WM functional abnormalities, extending the understanding of WM dysfunction's role in pathological mechanism of VCI.

CRediT authorship contribution statement

Juanwei Ma: Methodology, Software, Validation, Visualization, Writing – original draft. **Feng Liu:** Conceptualization, Funding acquisition, Methodology, Project administration, Software, Supervision, Validation, Writing – review & editing. **Yang Wang:** Data curation, Validation. **Lin Ma:** Methodology, Software, Visualization. **Yali Niu:** Data curation, Formal analysis. **Jing Wang:** Data curation. **Zhaoxiang Ye:** Supervision, Writing – review & editing. **Jing Zhang:** Conceptualization, Project administration, Writing – review & editing.

Declaration of Competing Interest

The authors declare that they have no known competing financial interests or personal relationships that could have appeared to influence the work reported in this paper.

Data availability

Data will be made available on request.

Acknowledgement

This work was supported by Natural Science Foundation of China (grant numbers: 82072001).

Appendix A. Supplementary data

Supplementary data to this article can be found online at https://doi.org/10.1016/j.nicl.2022.103245.

References

Ai, Q., Pu, Y.H., Sy, C., Liu, L.P., Gao, P.Y., 2014. Impact of regional white matter lesions on cognitive function in subcortical vascular cognitive impairment. Neurol. Res. 36 (5), 434–443. https://doi.org/10.1179/1743132814y.0000000354.

Ashburner, J., 2007. A fast diffeomorphic image registration algorithm. Neuroimage 38 (1), 95–113. https://doi.org/10.1016/j.neuroimage.2007.07.007.

Babalola, K.O., Patenaude, B., Aljabar, P., Schnabel, J., Kennedy, D., Crum, W., et al., 2009. An evaluation of four automatic methods of segmenting the subcortical structures in the brain. Neuroimage 47 (4), 1435–1447. https://doi.org/10.1016/j.neuroimage.2009.05.029.

Barker, R., Wellington, D., Esiri, M.M., Love, S., 2013. Assessing white matter ischemic damage in dementia patients by measurement of myelin proteins. J. Cereb. Blood Flow Metab. 33 (7), 1050–1057. https://doi.org/10.1038/jcbfm.2013.46.

Biswal, B., Yetkin, F.Z., Haughton, V.M., Hyde, J.S., 1995. Functional connectivity in the motor cortex of resting human brain using echo-planar MRI. Magn. Reson. Med. 34 (4), 537–541. https://doi.org/10.1002/mrm.1910340409.

Blumensath, T., Jbabdi, S., Glasser, M.F., Van Essen, D.C., Ugurbil, K., Behrens, T.E., Smith, S.M., 2013. Spatially constrained hierarchical parcellation of the brain with resting-state fMRI. Neuroimage 76, 313–324. https://doi.org/10.1016/j.neuroimage.2013.03.024.

Boyle, P.A., Yu, L., Fleischman, D.A., Leurgans, S., Yang, J., Wilson, R.S., et al., 2016. White matter hyperintensities, incident mild cognitive impairment, and cognitive decline in old age. Ann. Clin. Transl. Neurol. 3 (10), 791–800. https://doi.org/10.1002/acn3.343.

Chen, X., Zhang, H., Zhang, L., Shen, C., Lee, S.W., Shen, D., 2017. Extraction of dynamic functional connectivity from brain grey matter and white matter for MCI classification. Hum. Brain Mapp. 38 (10), 5019–5034. https://doi.org/10.1002/hbm.23711.

Chen, H.J., Gao, Y.Q., Che, C.H., Lin, H., Ruan, X.L., 2018. Diffusion tensor imaging with tract-based spatial statistics reveals white matter abnormalities in patients with vascular cognitive impairment. Front. Neuroanat. 12, 53. https://doi.org/10.3389/fnana.2018.00053.

Craddock, R.C., James, G.A., Holtzheimer 3rd, P.E., Hu, X.P., Mayberg, H.S., 2012. A whole brain fMRI atlas generated via spatially constrained spectral clustering. Hum. Brain Mapp. 33 (8), 1914–1928. https://doi.org/10.1002/hbm.21333.

Desikan, R.S., Ségonne, F., Fischl, B., Quinn, B.T., Dickerson, B.C., Blacker, D., et al., 2006. An automated labeling system for subdividing the human cerebral cortex on MRI scans into gyral based regions of interest. Neuroimage 31 (3), 968–980. https://doi.org/10.1016/j.neuroimage.2006.01.021.

Ding, Z., Huang, Y., Bailey, S.K., Gao, Y., Cutting, L.E., Rogers, B.P., Newton, A.T., Gore, J.C., 2018. Detection of synchronous brain activity in white matter tracts at rest and under functional loading. Proc. Natl. Acad. Sci. USA 115 (3), 595–600. https://doi.org/10.1073/pnas.1711567115.

Fan, Y.S., Li, Z., Duan, X., Xiao, J., Guo, X., Han, S., et al., 2020. Impaired interactions among white-matter functional networks in antipsychotic-naive first-episode schizophrenia. Hum. Brain Mapp. 41 (1), 230–240. https://doi.org/10.1002/hbm.24801.

Filley, C.M., Fields, R.D., 2016. White matter and cognition: making the connection. J. Neurophysiol. 116 (5), 2093–2104. https://doi.org/10.1152/jn.00221.2016.

Filley, C., 2012. The Behavioral Neurology of White Matter. OUP, New York.

Fox, M.D., Raichle, M.E., 2007. Spontaneous fluctuations in brain activity observed with functional magnetic resonance imaging. Nat. Rev. Neurosci. 8 (9), 700–711. https://doi.org/10.1038/nrn2201.

Friston, K.J., Williams, S., Howard, R., Frackowiak, R.S., Turner, R., 1996. Movement-related effects in fMRI time-series. Magn. Reson. Med. 35 (3), 346–355. https://doi.org/10.1002/mrm.1910350312.

Gao, Y., Sengupta, A., Li, M., Zu, Z., Rogers, B.P., Anderson, A.W., Ding, Z., Gore, J.C., 2020. Functional connectivity of white matter as a biomarker of cognitive decline in Alzheimer's disease. PLoS One 15 (10), e0240513.

Gore, J.C., Li, M., Gao, Y., Wu, T.L., Schilling, K.G., Huang, Y., et al., 2019. Functional MRI and resting state connectivity in white matter - a mini-review. Magn. Reson. Imaging 63, 1–11. https://doi.org/10.1016/j.mri.2019.07.017.

Guo, W., Liu, F., Liu, Z., Gao, K., Xiao, C., Chen, H., Zhao, J., 2012a. Right lateralized white matter abnormalities in first-episode, drug-naive paranoid schizophrenia. Neuroscience Letters. 531 (1), 5–9. https://doi.org/10.1016/j.neulet.2012.09.033.

Guo, W.B., Liu, F., Xue, Z.M., Gao, K., Wu, R.R., Ma, C.Q., et al., 2012b. Altered white matter integrity in young adults with first-episode, treatment-naive, and treatment-responsive depression. Neuroscience Letters. 522 (2), 139–144. https://doi.org/10.1016/j.neulet.2012.06.027.

Han, Y., Wang, J., Zhao, Z., Min, B., Lu, J., Li, K., He, Y., Jia, J., 2011. Frequency-dependent changes in the amplitude of low-frequency fluctuations in amnestic mild cognitive impairment: a resting-state fMRI study. Neuroimage 55 (1), 287–295. https://doi.org/10.1016/j.neuroimage.2010.11.059.

He, Z., Du, L., Huang, Y., Jiang, X., Lv, J., Guo, L., Zhang, S., Zhang, T., 2022. Gyral hinges account for the highest cost and the highest communication capacity in a Corticocortical network. Cereb. Cortex 32 (16), 3359–3376. https://doi.org/10.1093/cercor/bhab420.

Holland, P.R., Searcy, J.L., Salvadores, N., Scullion, G., Chen, G., Lawson, G., et al., 2015. Gliovascular disruption and cognitive deficits in a mouse model with features of small vessel disease. J. Cereb. Blood Flow Metab. 35 (6), 1005–1014. https://doi.org/10.1038/jcbfm.2015.12.

Iadecola, C., 2013. The pathobiology of vascular dementia. Neuron 80 (4), 844–866. https://doi.org/10.1016/j.neuron.2013.10.008.

Ji, G.J., Liao, W., Chen, F.F., Zhang, L., Wang, K.J.S.B., 2017. Low-frequency blood oxygen level-dependent fluctuations in the brain white matter: more than just noise. Sci. Bull. 62, 656–657. https://doi.org/10.1016/j.scib.2017.03.021.

Jiang, Y., Luo, C., Li, X., Li, Y., Yang, H., Li, J., et al., 2019a. White-matter functional networks changes in patients with schizophrenia. Neuroimage 190, 172–181. https://doi.org/10.1016/j.neuroimage.2018.04.018.

Jiang, Y., Song, L., Li, X., Zhang, Y., Chen, Y., Jiang, S., et al., 2019b. Dysfunctional white-matter networks in medicated and unmedicated benign epilepsy with centrotemporal spikes. Hum. Brain Mapp. 40 (10), 3113–3124. https://doi.org/10.1002/hbm.24584.

Kalaria, R.N., 2016. Neuropathological diagnosis of vascular cognitive impairment and vascular dementia with implications for Alzheimer's disease. Acta Neuropathol. 131 (5), 659–685. https://doi.org/10.1007/s00401-016-1571-z.

Kantarci, K., Murray, M.E., Schwarz, C.G., Reid, R.I., Przybelski, S.A., Lesnick, T., et al., 2017. White-matter integrity on DTI and the pathologic staging of Alzheimer's disease. Neurobiol. Aging 56, 172–179. https://doi.org/10.1016/j.neurobiolaging.2017.04.024.

Lange, T., Roth, V., Braun, M.L., Buhmann, J.M., 2004. Stability-based validation of clustering solutions. Neural Comput. 16 (6), 1299–1323. https://doi.org/10.1162/089976604773717621.

Levit, A., Hachinski, V., Whitehead, S.N., 2020. Neurovascular unit dysregulation, white matter disease, and executive dysfunction: the shared triad of vascular cognitive impairment and Alzheimer disease. Geroscience 42 (2), 445–465. https://doi.org/10.1007/s11357-020-00164-6.

Li, C., Liu, C., Yin, X., Yang, J., Gui, L., Wei, L., Wang, J., 2014. Frequency-dependent changes in the amplitude of low-frequency fluctuations in subcortical ischemic vascular disease (SIVD): a resting-state fMRI study. Behav. Brain Res. 274, 205–210. https://doi.org/10.1016/j.bbr.2014.08.019.

Li, M., Gao, Y., Gao, F., Anderson, A.W., Ding, Z., Gore, J.C., 2020. Functional engagement of white matter in resting-state brain networks. Neuroimage 220, 117096. https://doi.org/10.1016/j.neuroimage.2020.117096.

Li, M., Gao, Y., Ding, Z., Gore, J.C., 2021. Power spectra reveal distinct BOLD resting-state time courses in white matter. *Proc. Natl. Acad. Sci. USA* 118 (44). https://doi.org/10.1073/pnas.2103104118 e2103104118.

Li, X., Zhang, S., Jiang, X., Zhang, S., Han, J., Guo, L., Zhang, T., 2022. Cortical development coupling between surface area and sulcal depth on macaque brains. Brain Struct. Funct. 227 (3), 1013–1029. https://doi.org/10.1007/s00429-021-02444-z.

Lin, H., Sun, Y., Li, M., Zhan, Y., Lin, L., Ding, Z., Han, Y., 2020. Sex modulates the apolipoprotein E ε4 effect on white matter and cortical functional connectivity in individuals with amnestic mild cognitive impairment. Eur. J. Neurol. 27 (8), 1415–1421. https://doi.org/10.1111/ene.14226.

Liu, F., Guo, W., Liu, L., Long, Z., Ma, C., Xue, Z., et al., 2013. Abnormal amplitude low-frequency oscillations in medication-naive, first-episode patients with major depressive disorder: a resting-state fMRI study. J. Affect. Disord. 146 (3), 401–406. https://doi.org/10.1016/j.jad.2012.10.001.

Liu, F., Guo, W., Fouche, J.P., Wang, Y., Wang, W., Ding, J., et al., 2015. Multivariate classification of social anxiety disorder using whole brain functional connectivity. Brain Structure and Function. 220 (1), 101–115. https://doi.org/10.1007/s00429-013-0641-4.

Liu, F., Wang, Y., Li, M., Wang, W., Li, R., Zhang, Z., Lu, G., Chen, H., 2017. Dynamic functional network connectivity in idiopathic generalized epilepsy with generalized tonic-clonic seizure. Hum Brain Mapp. 38 (2), 957–973. https://doi.org/10.1002/hbm.23430.

Logothetis, N.K., Pauls, J., Augath, M., Trinath, T., Oeltermann, A., 2001. Neurophysiological investigation of the basis of the fMRI signal. Nature 412 (6843), 150–157. https://doi.org/10.1038/35084005.

Lorio, S., Fresard, S., Adaszewski, S., Kherif, F., Chowdhury, R., Frackowiak, R.S., et al., 2016. New tissue priors for improved automated classification of subcortical brain structures on MRI. Neuroimage 130, 157–166. https://doi.org/10.1016/j.neuroimage.2016.01.062.

Lu, F., Cui, Q., He, Z., Tang, Q., Chen, Y., Sheng, W., et al., 2021. Superficial white-matter functional networks changes in bipolar disorder patients during depressive episodes. J. Affect. Disord. 289, 151–159. https://doi.org/10.1016/j.jad.2021.04.029.

Ma, L., Liu, M., Xue, K., Ye, C., Man, W., Cheng, M., et al., 2022. Abnormal regional spontaneous brain activities in white matter in patients with autism spectrum disorder. Neuroscience 490, 1–10. https://doi.org/10.1016/j.neuroscience.2022.02.022.

Makedonov, I., Black, S.E., Macintosh, B.J., 2013. BOLD fMRI in the white matter as a marker of aging and small vessel disease. PLoS One 8 (7), e67652.

Makedonov, I., Chen, J.J., Masellis, M., MacIntosh, B.J., 2016. Physiological fluctuations in white matter are increased in Alzheimer's disease and correlate with neuroimaging and cognitive biomarkers. Neurobiol. Aging 37, 12–18. https://doi.org/10.1016/j.neurobiolaging.2015.09.010.

Mascalchi, M., Salvadori, E., Toschi, N., Giannelli, M., Orsolini, S., Ciulli, S., et al., 2019. DTI-derived indexes of brain WM correlate with cognitive performance in vascular MCI and small-vessel disease. A TBSS study. *Brain Imaging Behav.* 13 (3), 594–602. https://doi.org/10.1007/s11682-018-9873-5.

Masumura, M., Hata, R., Nagai, Y., Sawada, T., 2001. Oligodendroglial cell death with DNA fragmentation in the white matter under chronic cerebral hypoperfusion: comparison between normotensive and spontaneously hypertensive rats. Neurosci. Res. 39 (4), 401–412. https://doi.org/10.1016/s0168-0102(01)00195-x.

Min, B.K., Hämäläinen, M.S., Pantazis, D., 2020. New cognitive neurotechnology facilitates studies of cortical-subcortical interactions. Trends Biotechnol. 38 (9), 952–962. https://doi.org/10.1016/j.tibtech.2020.03.003.

Mungas, D., Jagust, W.J., Reed, B.R., Kramer, J.H., Weiner, M.W., Schuff, N., et al., 2001. MRI predictors of cognition in subcortical ischemic vascular disease and Alzheimer's disease. Neurology 57 (12), 2229–2235. https://doi.org/10.1212/wnl.57.12.2229.

O'Brien, J.T., Erkinjuntti, T., Reisberg, B., Roman, G., Sawada, T., Pantoni, L., et al., 2003. Vascular cognitive impairment. Lancet Neurol. 2 (2), 89–98. https://doi.org/10.1016/s1474-4422(03)00305-3.

Peer, M., Nitzan, M., Bick, A.S., Levin, N., Arzy, S., 2017. Evidence for functional networks within the human brain's white matter. J. Neurosci. 37 (27), 6394–6407. https://doi.org/10.1523/jneurosci.3872-16.2017.

Pendlebury, S.T., Cuthbertson, F.C., Welch, S.J., Mehta, Z., Rothwell, P.M., 2010. Underestimation of cognitive impairment by Mini-Mental State Examination versus the Montreal Cognitive Assessment in patients with transient ischemic attack and stroke: a population-based study. Stroke 41 (6), 1290–1293. https://doi.org/10.1161/strokeaha.110.579888.

Qin, Q., Tang, Y., Dou, X., Qu, Y., Xing, Y., Yang, J., Chu, T., Liu, Y., Jia, J., 2021. Default mode network integrity changes contribute to cognitive deficits in subcortical vascular cognitive impairment, no dementia. Brain Imaging Behav. 15 (1), 255–265. https://doi.org/10.1007/s11682-019-00252-y.

Reimer, M.M., McQueen, J., Searcy, L., Scullion, G., Zonta, B., Desmazieres, A., et al., 2011. Rapid disruption of axon-glial integrity in response to mild cerebral hypoperfusion. J. Neurosci. 31 (49), 18185–18194. https://doi.org/10.1523/jneurosci.4936-11.2011.

Salvador, R., Suckling, J., Schwarzbauer, C., Bullmore, E., 2005. Undirected graphs of frequency-dependent functional connectivity in whole brain networks. Philos. Trans. R. Soc. Lond. B Biol. Sci. 360 (1457), 937–946. https://doi.org/10.1098/rstb.2005.1645.

Schaefer, A., Kong, R., Gordon, E.M., Laumann, T.O., Zuo, X.N., Holmes, A.J., Eickhoff, S. B., Yeo, B.T.T., 2018. Local-global parcellation of the human cerebral cortex from intrinsic functional connectivity MRI. Cereb. Cortex 28 (9), 3095–3114. https://doi.org/10.1093/cercor/bhx179.

Thong, J.Y., Du, J., Ratnarajah, N., Dong, Y., Soon, H.W., Saini, M., et al., 2014. Abnormalities of cortical thickness, subcortical shapes, and white matter integrity in subcortical vascular cognitive impairment. Hum. Brain Mapp. 35 (5), 2320–2332. https://doi.org/10.1002/hbm.22330.

Tournier, J.D., Calamante, F., Gadian, D.G., Connelly, A., 2004. Direct estimation of the fiber orientation density function from diffusion-weighted MRI data using spherical deconvolution. Neuroimage 23 (3), 1176–1185. https://doi.org/10.1016/j.neuroimage.2004.07.037.

Trigiani, L.J., Lacalle-Aurioles, M., Bourourou, M., Li, L., Greenhalgh, A.D., Zarruk, J.G., David, S., Fehlings, M.G., Hamel, E., 2020. Benefits of physical exercise on cognition and glial white matter pathology in a mouse model of vascular cognitive impairment and dementia. Glia 68 (9), 1925–1940. https://doi.org/10.1002/glia.23815.

Tu, M.C., Lo, C.P., Huang, C.F., Hsu, Y.H., Huang, W.H., Deng, J.F., Lee, Y.C., 2017. Effectiveness of diffusion tensor imaging in differentiating early-stage subcortical ischemic vascular disease, Alzheimer's disease and normal ageing. PLoS One 12 (4), e0175143.

Tuladhar, A.M., van Dijk, E., Zwiers, M.P., van Norden, A.G., de Laat, K.F., Shumskaya, E., Norris, D.G., de Leeuw, F.E., 2016. Structural network connectivity and cognition in cerebral small vessel disease. Hum. Brain Mapp. 37 (1), 300–310. https://doi.org/10.1002/hbm.23032.

van der Flier, W.M., Skoog, I., Schneider, J.A., Pantoni, L., Mok, V., Chen, C.L.H., Scheltens, P., 2018. Vascular cognitive impairment. Nat. Rev. Dis. Primers 4, 18003. https://doi.org/10.1038/nrdp.2018.3.

Wang, P., Meng, C., Yuan, R., Wang, J., Yang, H., Zhang, T., et al., 2020. The organization of the human corpus callosum estimated by intrinsic functional connectivity with white-matter functional networks. Cereb. Cortex 30 (5), 3313–3324. https://doi.org/10.1093/cercor/bhz311.

Woodward, N.D., Cascio, C.J., 2015. Resting-State Functional Connectivity in Psychiatric Disorders. JAMA Psychiatry. 72 (8), 743–744. https://doi.org/10.1001/jamapsychiatry.2015.0484.

Xue, K., Liang, S., Yang, B., Zhu, D., Xie, Y., Qin, W., Liu, F., Zhang, Y., Yu, C., 2020. Local dynamic spontaneous brain activity changes in first-episode, treatment-naïve patients with major depressive disorder and their associated gene expression profiles. Psychol Med. 1–10 https://doi.org/10.1017/s0033291720003876.

Yang, H., Long, X.Y., Yang, Y., Yan, H., Zhu, C.Z., Zhou, X.P., Zang, Y.F., Gong, Q.Y., 2007. Amplitude of low frequency fluctuation within visual areas revealed by resting-state functional MRI. Neuroimage 36 (1), 144–152. https://doi.org/10.1016/j.neuroimage.2007.01.054.

Yeo, B.T., Krienen, F.M., Sepulcre, J., Sabuncu, M.R., Lashkari, D., Hollinshead, M., et al., 2011. The organization of the human cerebral cortex estimated by intrinsic functional connectivity. J. Neurophysiol. 106 (3), 1125–1165. https://doi.org/10.1152/jn.00338.2011.

Yeo, B.T., Krienen, F.M., Chee, M.W., Buckner, R.L., 2014. Estimates of segregation and overlap of functional connectivity networks in the human cerebral cortex. Neuroimage 88, 212–227. https://doi.org/10.1016/j.neuroimage.2013.10.046.

Zalesky, A., Fornito, A., Bullmore, E.T., 2010. Network-based statistic: identifying differences in brain networks. Neuroimage 53 (4), 1197–1207. https://doi.org/10.1016/j.neuroimage.2010.06.041.

Zamboni, G., Griffanti, L., Jenkinson, M., Mazzucco, S., Li, L., Küker, W., Pendlebury, S. T., Rothwell, P.M., 2017. White matter imaging correlates of early cognitive impairment detected by the montreal cognitive assessment after transient ischemic attack and minor stroke. Stroke 48 (6), 1539–1547. https://doi.org/10.1161/strokeaha.116.016044.

Zhang, Z., Liao, W., Chen, H., Mantini, D., Ding, J.R., Xu, Q., et al., 2011. Altered functional-structural coupling of large-scale brain networks in idiopathic generalized epilepsy. Brain 134 (Pt 10), 2912–2928. https://doi.org/10.1093/brain/awr223.

Zhang, T., Chen, H., Guo, L., Li, K., Li, L., Zhang, S., Shen, D., Hu, X., Liu, T., 2014. Characterization of U-shape streamline fibers: methods and applications. Med. Image Anal. 18 (5), 795–807. https://doi.org/10.1016/j.media.2014.04.005.

Zhang, S., Chavoshnejad, P., Li, X., Guo, L., Jiang, X., Han, J., et al., 2022. Gyral peaks: Novel gyral landmarks in developing macaque brains. Hum. Brain Mapp. 43 (15), 4540–4555. https://doi.org/10.1002/hbm.25971.

Zou, Q.H., Zhu, C.Z., Yang, Y., Zuo, X.N., Long, X.Y., Cao, Q.J., Wang, Y.F., Zang, Y.F., 2008. An improved approach to detection of amplitude of low-frequency fluctuation (ALFF) for resting-state fMRI: fractional ALFF. J. Neurosci. Methods 172 (1), 137–141. https://doi.org/10.1016/j.jneumeth.2008.04.012.

Zuo, X.N., Di Martino, A., Kelly, C., Shehzad, Z.E., Gee, D.G., Klein, D.F., Castellanos, F. X., Biswal, B.B., Milham, M.P., 2010. The oscillating brain: complex and reliable. Neuroimage 49 (2), 1432–1445. https://doi.org/10.1016/j.neuroimage.2009.09.037.